7818 *Inorg. Chem.* **2009**, *48*, 7818–7827
DOI: 10.1021/ic900741y

Inorganic Chemistry
Article

Closo versus *Hypercloso* Metallaboranes: A DFT Study

Oottikkal Shameema[†] and Eluvathingal D. Jemmis*[,†,‡]

[†]*Department of Inorganic and Physical Chemistry, Indian Institute of Science, Bangalore -12, India, and* [‡]*Indian Institute of Science Education and Research Thiruvananthapuram, CET Campus, Thiruvananthapuram, Kerala, India 695016*

Received April 16, 2009

The structures and electronic relationship of 9-, 10-, 11-, and 12-vertex *closo* and *hypercloso* (*isocloso*) metallaboranes are explored using DFT calculations. The role of the transition metal in stabilizing the *hypercloso* borane structures is explained using the concept of orbital compatibility. The *hypercloso* structures, $C_6H_6MB_{n-1}H_{n-1}$ (n = 9−12; M = Fe, Ru, and Os) are taken as model complexes. Calculations on metal free polyhedral borane B_nH_n suggest that n vertex *hypercloso* structures need only n skeleton electron pairs (SEPs), but the structure will have one or more six-degree vertices, whereas the corresponding *closo* structures with n + 1 SEPs have only four- and five-degree vertices. This high-degree vertex of *hypercloso* structures can be effectively occupied by transition metal fragments with their highly diffused orbitals. Calculations further show that a heavy transition metal with more diffused orbitals prefers over a light transition metal to form *hypercloso* geometry. This is in accordance with the fact that there are more experimentally characterized *hypercloso* structures with the heavy transition metals. The size of the exohedral ligands attached to the metal atom also plays a role in deciding the stability of the *hypercloso* structure. The interaction between the borane and the metal fragments in the *hypercloso* geometry is analyzed using the fragment molecular orbital approach. The interconversion of the *closo* and *hypercloso* structures by the addition and removal of the electrons is also discussed in terms of the correlation diagrams.

Introduction

The *closo* polyhedral boranes have long been of great theoretical and experimental interest.[1] The most stable polyhedral *closo* boranes are based on the spherical deltahedra. The Wade's $n + 1$ rule[2] forms the basis for the special stability of such spherical deltahedra with two negative charges, $B_nH_n^{2-}$, due to their three-dimensional aromaticity. The replacement of BH fragments by isolobal transition metal fragments[3] in the polyhedral boranes gives stable metallaboranes, which can also follow various electron counting rules. For example, the metallacarborane, $CpCoC_2B_9H_{11}$ (**1**, Figure 1), where one of the BH fragments of icosahedral $C_2B_{10}H_{12}$ is replaced by the isolobal $(C_5H_5)Co$ fragment, obeys Wade's rule.[4] Early examples of metallaboranes were found to adopt structures which are analogous to that of boranes and carboranes. Metal fragments in these complexes are regarded as contributing three orbitals and two electrons toward the cluster bonding. However, even when the electron counting rules were formulated, exceptions in terms of either structure or electron counts were recognized, and many more are known now.[5] These include neutral boron halides[6] such as B_8Cl_8 and B_9Cl_9 and many metallaboranes.[7]

In 1975, Hawthorne and co-workers[8] reported the synthesis and structural characterization of a 10-vertex metallacarborane, η^5-$Cp_2Fe_2C_2B_6H_8$ (**2**, Figure 1). They noted that the structure adopted by this cluster, which has only 10 skeleton electron pairs (SEPs), is geometrically different from

*To whom correspondence should be addressed. E-mail: jemmis@iisertvm.ac.in.

(1) (a) Stock, A. *Hydrides of Boron and Silicon*; Cornell University Press: Ithaca, NY, 1933. (b) Williams, R. E. *Inorg. Chem.* **1971**, *10*, 210.

(2) (a) Wade, K. *Chem. Commun.* **1971**, 792. (b) Wade, K. *Electron Deficient Compounds*; Nelson: London, 1971. (c) Olah, G. A.; Wade, K.; Williams, R. E. *Electron Deficient Boron and Carbon Clusters*; Wiley: New York, 1991.

(3) Hoffmann, R. *Angew. Chem., Int. Ed.* **1982**, *21*, 711.

(4) (a) Rudolph, R. W. *Acc. Chem. Res.* **1976**, *9*, 446. (b) Mingos, D. M. P. *Acc. Chem. Res.* **1984**, *17*, 311.

(5) (a) Aihara, J. *Bull. Chem. Soc. Jpn.* **1983**, *56*, 335. (b) Fowler, P. W. *Polyhedron* **1985**, *4*, 2051. (c) Kennedy, J. D. In *The Borane-Carborane-Carbocation Continuum*; Casanova, J., Ed.; Wiley: New York, 1998; p 85. (d) Peymann, T.; Knobler, C. B.; Khan, S. I.; Hawthorne, M. F. *Angew. Chem., Int. Ed.* **2001**, *40*, 1664.

(6) (a) Morrison, J. A. *Chem. Rev.* **1991**, *91*, 35. (b) LeBreton, P. R.; Urano, S.; Shahbaz, M.; Emery, S. L.; Morrison, J. A. *J. Am. Chem. Soc.* **1986**, *108*, 3937. (c) Swanton, D. J.; Ahlrichs, R.; Häser, M. *Chem. Phys. Lett.* **1989**, *155*, 329. (d) Hönle, W.; Grin, Y.; Burkhardt, A.; Wedig, U.; Schultheiss, M.; von Schnering, H. G. *J. Solid State Chem.* **1997**, *133*, 59.

(7) (a) *Advances in Boron Chemistry*; Siebert, W., Ed.; Royal Society of Chemistry: Cambridge, U.K., 1997. (b) *The Borane-Carborane-Carbocation Continuum*; Casanova, J., Ed.; Wiley: New York, 1998. (c) Ghosh, S.; Shang, M.; Li, Y.; Fehlner, T. P. *Angew. Chem., Int. Ed.* **2001**, *40*, 1125. (d) Wadepohl, H. *Angew. Chem., Int. Ed.* **2002**, *41*, 4220.

(8) Callahan, K. P.; Evans, W. J.; Lo, F. Y.; Strouse, C. E.; Hawthorne, M. F. *J. Am. Chem. Soc.* **1975**, *97*, 296.

 Published on Web 07/14/2009

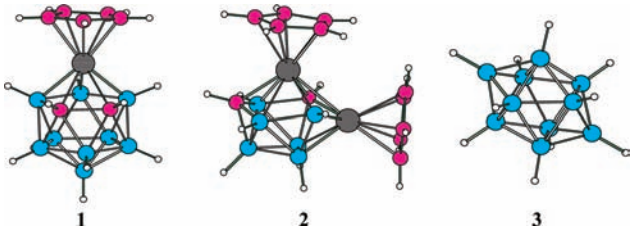

Figure 1. Experimentally characterized structures of η^5-$CpCoC_2B_9H_{11}$ (**1**), η^5-$Cp_2Fe_2C_2B_6H_8$ (**2**), and $B_{10}H_{10}^{2-}$ (**3**).

that of the metal free polyhedral boranes, $B_{10}H_{10}^{2-}$ (**3**, Figure 1). Hawthorne subsequently characterized a 10-vertex, electron-deficient mono metallaborane with 10 SEPs, $[Ru\{PPh_2C_6H_4(CH_2CH{=}CH_2)\text{-}2\}(\eta^6\text{-}C_2B_7H_7Me_2)]$,[9] and introduced the term *hypercloso* (implying that there is an enhanced electron deficiency in the cluster). The term has gained general acceptance to describe electron-deficient *closo* systems such as neutral B_nH_n cages and their derivatives.[10] On the basis of electron counting arguments and by comparison to the known structural analogues, Baker[11] suggested that these complexes contain two skeletal electrons fewer than their *closo* counterparts and are thus best regarded as *hypercloso* metallaboranes.

Further development of metallaboranes, especially through the work of Kennedy et al.[12] and Fehlner et al.,[13] led to the synthesis of a variety of metallaboranes which cannot be explained by Wade's rule. Kennedy and co-workers treated the metal fragment as a four orbital−four electron donor toward cluster bonding so that the metal fragment donates an additional electron pair. This again brings the SEP count of the cluster to $n + 1$. Since number of SEPs is the same as that of the *closo* structure, they considered these clusters to be the isomer of the *closo* structure, that is, *isocloso*.[12b,14] According to them, electron deficiency is located on the metal, so that the metal forms a 16-electron complex.[14b] Johnston and Mingos[15] have shown, using molecular orbital calculations with the extended Hückel method, that the distortions from *closo* to *hypercloso* increase the connectivity of the metal atom with borane, which provides additional stability. They further pointed out that, since these compounds with *n* SEPs are electron-deficient with respect to the *closo* structures with an $n+1$ electron count, the term *hypercloso* is more appropriate. Using the bonding topology, King[16] has shown that, in these metallaboranes, the metal

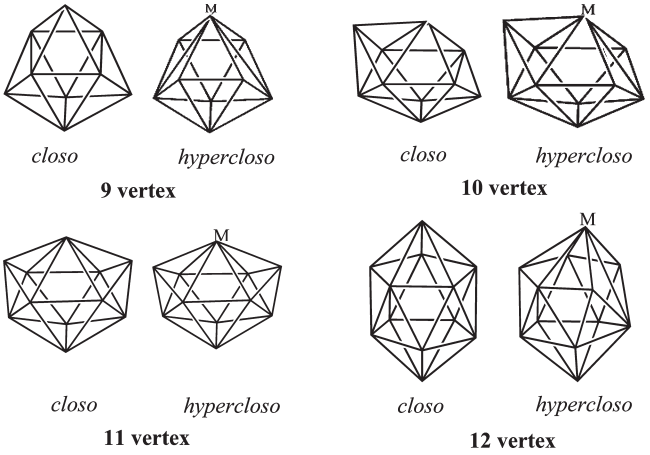

Figure 2. The 9-, 10-, 11-, and 12-vertex *closo* and *hypercloso* structures.

Figure 3. Schematic representation showing the interconversion of 10-vertex *closo* to *hypercloso* geometry through an *isonido* intermediate.

vertices contribute three orbitals and two electrons toward cluster bonding. They have also shown[17] that, while going from the *closo* to the *hypercloso* structure, the metal oxidation state increases by two through the internal metal oxidative addition reactions, but the metal valence electron count remains the same. Since there is an ambiguity in the electronic structure of *hypercloso* metallaboranes, we choose to carry out DFT calculations to explore the structure and electronic relationship of *closo* and *hypercloso* metallaboranes.

The *closo* and *hypercloso* pair of a given vertex system differ both in topology and in SEP (Figure 2). Among these *hypercloso* metallaboranes, the 9- and 10-vertex mono metallaboranes have one six-degree vertex (the degree of a vertex refers to the number of boron atoms connected to it) occupied by a transition metal fragment, whereas the corresponding metal-free deltahedra have only four- and five-degree vertices. Both the *closo* and *hypercloso* structures of 11-vertex clusters with one six-degree vertex are topologically equivalent but electronically different. The topological impossibility of an 11-vertex deltahedron to have only four- and five-degree vertices makes both the *closo* and *hypercloso* 11-vertex structures topologically equivalent.[18] The 12-vertex *hypercloso* metallaborane has two six-degree vertices, whereas the corresponding *closo* metallaborane has five-degree vertices only.

Hypercloso structures can be derived from the corresponding *closo* structures by the diamond−square−diamond rearrangement (DSD; Figure 3), which is the mechanism for framework rearrangement[19] in boranes and carboranes. In

(9) Jung, C. W.; Baker, R. T.; Hawthorne, M. F. *J. Am. Chem. Soc.* **1981**, *103*, 810.
(10) (a) McKee, M. L. *Inorg. Chem.* **1999**, *38*, 321. (b) McKee, M. L.; Wang, Z.-X.; Schleyer, P. v. R. *J. Am. Chem. Soc.* **2000**, *122*, 4781.
(11) Baker, R. T. *Inorg. Chem.* **1986**, *25*, 109.
(12) (a) Bould, J.; Greenwood, N. N.; Kennedy, J. D. *J. Chem. Soc., Dalton Trans.* **1990**, 1451. (b) Bould, J.; Kennedy, J. D.; Thornton-Pett, M. *J. Chem. Soc., Dalton Trans.* **1992**, 563. (c) Stibr, B.; Kennedy, J. D.; Drdakova, E.; Thornton-Pett, M. *J. Chem. Soc., Dalton Trans.* **1994**, 229.
(13) (a) Kawamura, K.; Shang, M.; Wiest, O.; Fehlner, T. P. *Inorg. Chem.* **1998**, *37*, 608. (b) Weller, A. S.; Shang, M.; Fehlner, T. P. *Organometallics* **1999**, *18*, 853. (c) Fehlner, T. P. *J. Organomet. Chem.* **2009**, *694*, 1671.
(14) (a) Kennedy, J. D. *Inorg. Chem.* **1986**, *25*, 111. (b) Crook, J. E.; Elrington, M.; Greenwood, N. N.; Kennedy, J. D.; Woollins, J. D. *Polyhedron* **1984**, *3*, 901.
(15) (a) Johnston, R. L.; Mingos, D. M. P. *Inorg. Chem.* **1986**, *25*, 3321. (b) Johnston, R. L.; Mingos, D. M. P. *Polyhedron* **1986**, *5*, 2059. (c) Johnston, R. L.; Mingos, D. M. P. *J. Chem. Soc., Dalton Trans.* **1987**, 647. (d) Johnston, R. L.; Mingos, D. M. P; Sherwood, P. *New. J. Chem.* **1991**, *15*, 831.
(16) (a) King, R. B. *Inorg. Chem.* **1999**, *38*, 5151. (b) King, R. B. *Inorg. Chem.* **2006**, *45*, 8211. (c) King, R. B. *J. Organomet. Chem.* **2009**, *694*, 1602.
(17) King, R. B.; Hagel, J. *Polyhedron* **2006**, *25*, 3183.
(18) King, R. B.; Duijvestijn, A. J. W. *Inorg. Chim. Act.* **1990**, *178*, 55.
(19) (a) Lipscomb, W. N. *Science.* **1966**, *153*, 3734. (b) Kennedy, J. D. In *Progress in Inorganic Chemistry*; Wiley: New York, 1986; Vol. *34*. (c) Gimarc, B. M.; Warren, D. S.; Brown; Ott, J. J.; Borwn, C. *Inorg. Chem.* **1991**, *30*, 1598. (d) McKee, M. L. *J. Am. Chem. Soc.* **1995**, *117*, 8001. (e) Wales, D. J.; Bone, R. G. A. *J. Am. Chem. Soc.* **1992**, *114*, 5399. (f) Zhao, M.; Gimarc, B. M. *Polyhedron* **1995**, *14*, 1315. (g) McKee, M. L. *J. Am. Chem. Soc.* **1992**, *114*, 879. (h) Shameema, O.; Pathak, B.; Jemmis, E. D. *Inorg. Chem.* **2008**, *47*, 4375.

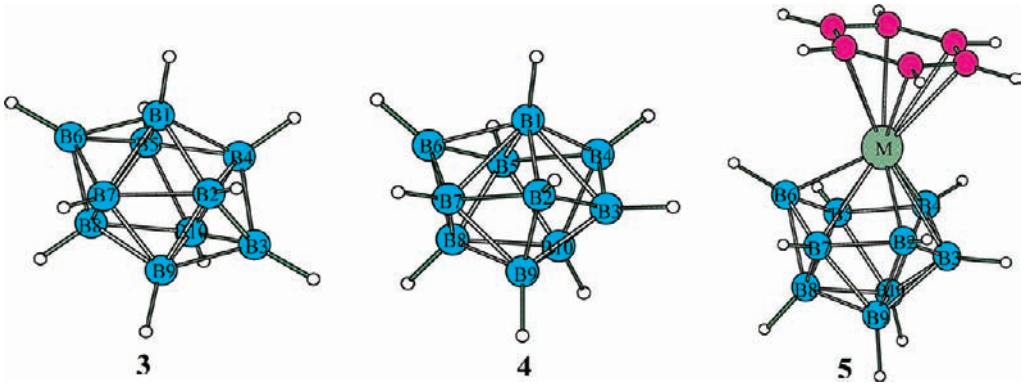

Figure 4. The optimized structure of *closo* $B_{10}H_{10}^{2-}$ (**3**); *hypercloso* $B_{10}H_{10}$ (**4**); and *hypercloso* $C_6H_6MB_9H_9$, M = Fe, Ru, and Os (**5**).

such a DSD rearrangement, the intermediate polyhedron with a single quadrilateral face looks like a *nido* structure. This is called an *isonido* structure. The removal of the lowest degree vertex from the $n + 1$ vertex *closo* polyhedron also gives an *isonido* structure. This is in contrast to the fact that the classical *nido* structures are obtained by the removal of the highest degree vertex from the corresponding *closo* structure. Similarly, the removal of the lowest degree vertex from the *isonido* structure gives the *isoarachno* structure. The synthesis and characterization of many *isonido* clusters with a range of metal atoms and ligand combinations have been reported in the literature.[20] There are a few examples for the isolation and characterization of the *isoarachno* structures.[21]

Here, we analyze with DFT calculations the structure and electronic relationship of the *closo* and *hypercloso* pair for parent borane systems (B_nH_n) where $n = 9-12$. These relationships will be compared with that of the *closo* and *hypercloso* metallaboranes. The role of the transition metal in stabilizing the *hypercloso* geometry will be explored, taking the *hypercloso* mono metallaboranes, $C_6H_6MB_{n-1}H_{n-1}$ ($n = 9-12$; M = Fe, Ru, and Os) as model complexes. The interconversion of *closo* and *hypercloso* structures on the addition and removal of electrons for both the boranes and the metallaboranes will be discussed. It is interesting to investigate the factors that drive the equilibrium between a *closo* and a *hypercloso* structure, within a given vertex system. The influence of the size of the metal atom and nature of the exohedral ligands on the stability of the metallaboranes in *hypercloso* geometry also will be explored.

Computational Methods

The geometries of all metallaborane structures are optimized using the hybrid[22] HF-DFT method B3LYP/LANL2DZ. The B3LYP[22a,22b] method is based on Becke's three-parameter functional including the Hartree−Fock exchange contribution with a nonlocal correction for the exchange potential proposed by Becke, together with the nonlocal correction for the correlation energy suggested by Lee et al. The LANL2DZ[22c] basis set uses the effective core potential of Hay and Wadt. The borane clusters are optimized at the B3LYP/6-31G* level of calculation. The interaction diagram is obtained from the extended Hückel calculation using CACAO[22d] on B3LYP optimized structures. The nature of stationary points is characterized by vibrational frequency calculations. All optimizations are carried out using the Gaussian 03 suite of programs.[23]

Results and Discussion

We begin the analysis by describing the structure and bonding of the *closo*−*hypercloso* pair of 10-vertex borane. The *closo* $B_{10}H_{10}^{2-}$ (D_{4d}) with 11 SEPs has a square-planar antiprismatic geometry (**3**, Figure 4) with eight five-degree and two four-degree vertices. The *hypercloso* $B_{10}H_{10}$ (C_{3v}) with 10 SEPs has one six-degree (B1), six five-degree, and three four-degree vertices (**4**, Figure 4). Optimization of the *hypercloso* $B_{10}H_{10}$ (**4**), after the addition of two electrons, converges into the *closo* structure (**3**). Similarly removing two electrons from *closo* $B_{10}H_{10}^{2-}$ (**3**) converts the structure into the *hypercloso* geometry (**4**). It implies that a $B_{10}H_{10}$ cluster is stable in *hypercloso* geometry with 10 SEPs and *closo* geometry with 11 SEPs.

The *hypercloso* structure (**4**) can be derived from the corresponding *closo* structure (**3**) by DSD rearrangement

(20) (a) Greenwood, N. N.; Kennedy, J. D. *Pure. Appl. Chem.* **1991**, *63*, 317. (b) Hwang, J.-W.; Kim, J.-H.; Lee, H.; Lee, H.; Kim, S.; Kwak, J.; Do, Y. *J. Am. Chem. Soc.* **2001**, *123*, 9054. (c) Rosair, G. M.; Welch, A. J.; Weller, A. S. *Organometallics* **1998**, *17*, 3227. (d) McWhannell, M. A.; Rosair, G. M.; Welch, A. J.; Teixidor, F.; Vinas, C. *J. Organomet. Chem.* **1999**, *573*, 165. (e) Teixidor, F.; Vinas, C.; Flores, M. A.; Rosair, G. M.; Welch, A. J.; Weller, A. S. *Inorg. Chem.* **1998**, *37*, 5394. (f) Garrioch, R. M.; Rosair, G. M.; Welch, A. J. *J. Organomet. Chem.* **2000**, *614*, 153. (g) Bould, J.; Clegg, W.; Spalding, T. R.; Kennedy, J. D. *Inorg. Chem. Commun.* **1999**, *2*, 315.

(21) (a) Bown, M.; Fontaine, X. L. R.; Greenwood, N. N.; Kennedy, J. D.; MacKinnon, P. *J. Chem. Soc., Chem. Commun.* **1987**, 817. (b) Ditzel, E. J.; Fontaine, X. L. R.; Greenwood, N. N.; Kennedy, J. D.; Sisan, Z.; Stibr, B.; Thornton-Pett, M. *J. Chem. Soc., Chem. Commun.* **1990**, 1741.

(22) (a) Becke, A. D. *Phys. Rev. A: At., Mol., Opt. Phys.* **1988**, *38*, 3098. (b) Lee, C.; Yang, W.; Parr, R. G. *Phys. Rev. B: Condens. Matter Mater. Phys.* **1988**, *37*, 785. (c) Hay, P. J.; Wadt, W. R. *J. Chem. Phys.* **1985**, *82*, 270. (d) Mealli, C.; Proserpio, D. M. *J. Chem. Educ.* **1990**, *67*, 399.

(23) Frisch, M. J.; Trucks, G. W.; Schlegel, H. B.; Scuseria, G. E.; Robb, M. A.; Cheeseman, J. R.; Montgomery, J. A., Jr.; Vreven, T.; Kudin, K. N.; Burant, J. C.; Millam, J. M.; Iyengar, S. S.; Tomasi, J.; Barone, V.; Mennucci, B.; Cossi, M.; Scalmani, G.; Rega, N.; Petersson, G. A.; Nakatsuji, H.; Hada, M.; Ehara, M.; Toyota, K.; Fukuda, R.; Hasegawa, J.; Ishida, M.; Nakajima, T.; Honda, Y.; Kitao, O.; Nakai, H.; Klene, M.; Li, X.; Knox, J. E.; Hratchian, H. P.; Cross, J. B.; Bakken, V.; Adamo, C.; Jaramillo, J.; Gomperts, R.; Stratmann, R. E.; Yazyev, O.; Austin, A. J.; Cammi, R.; Pomelli, C.; Ochterski, J. W.; Ayala, P. Y.; Morokuma, K.; Voth, G. A.; Salvador, P.; Dannenberg, J. J.; Zakrzewski, V. G.; Dapprich, S.; Daniels, A. D.; Strain, M. C.; Farkas, O.; Malick, D. K.; Rabuck, A. D.; Raghavachari, K.; Foresman, J. B.; Ortiz, J. V.; Cui, Q.; Baboul, A. G.; Clifford, S.; Cioslowski, J.; Stefanov, B. B.; Liu, G.; Liashenko, A.; Piskorz, P.; Komaromi, I.; Martin, R. L.; Fox, D. J.; Keith, T.; Al-Laham, M. A.; Peng, C. Y.; Nanayakkara, A.; Challacombe, M.; Gill, P. M. W.; Johnson, B.; Chen, W.; Wong, M. W.; Gonzalez, C.; Pople, J. A. *Gaussian 03*, revision B.03; Gaussian, Inc.: Pittsburgh, PA, 2003.

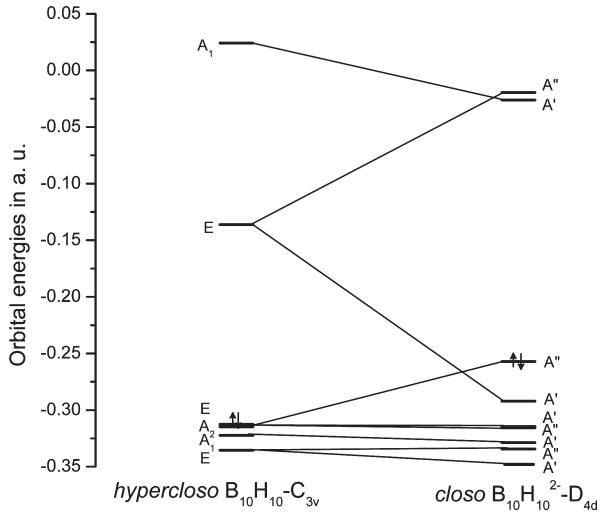

Figure 5. Correlation diagram for the interconversion of the *hypercloso*−*closo* structure for $B_{10}H_{10}$.

involving boron atoms B1, B2, B3, and B4 (**3**, Figure 4). In the *hypercloso* geometry (**4**), the B1−B3 and B2−B4 distances are 2.02 and 2.91 Å, respectively. In the *closo* geometry, the B1−B3 bond is lengthened to 2.92 Å and the B2−B4 bond is shortened to 1.84 Å. We have computed the correlation diagram for the interconversion of *hypercloso*−*closo* systems for the $B_{10}H_{10}$ cluster, as shown in Figure 5. In the *hypercloso* $B_{10}H_{10}$, both the HOMO and the LUMO are doubly degenerated. The LUMO (I, Figure 6a) of *hypercloso* geometry has a bonding interaction between B2 and B4 and an antibonding interaction between B1 and B3. The LUMO (II) has a bonding interaction between B1 and B3 and an antibonding interaction between B2 and B4. Thus, when we add two electrons, they are going to the LUMO (I) orbital, which gets stabilized while LUMO (II) gets destabilized (Figure 5). This results in the shortening of the B2−B4 bond and the lengthening of the B1−B3 bond, converting the *hypercloso* geometry to the *closo* geometry. The HOMO−1 orbital of the *hypercloso* geometry, which has an antibonding interaction between B2 and B4, is also getting destabilized as the B2−B4 distance decreases. Thus the LUMO (I) of the *hypercloso* geometry becomes the HOMO−1 of the *closo* geometry. The HOMO−1 of the *hypercloso* geometry becomes the HOMO of the *closo* geometry.

Even though $B_{10}H_{10}$ is a minimum in the *hypercloso* geometry, it has an unusual topology with one of the boron atoms (B1) at a six-degree vertex. In the *hypercloso* geometry, a BH group is capping a six-membered ring of the B_9H_9 fragment, whereas in *closo* geometry, it is capping a five-membered ring of the B_9H_9 fragment. According to the orbital compatibility,[24] the BH cap with the less diffused orbital is less compatible with overlapping with the six-membered ring orbitals of the B_9H_9 fragment, resulting in a less stable *hypercloso* structure of $B_{10}H_{10}$.

Stabilization of the *Hypercloso* Structures with the Transition Metal Fragments. The *hypercloso* geometry can be stabilized by substituting the BH vertex, which caps the six-membered ring of the B_9H_9 fragment, with a cap with more diffused orbitals. A transition metal fragment with more diffused orbitals can stabilize the *hypercloso* structure, which is reflected in the experimental synthesis of many *hypercloso* metallaboranes. A large number of *hypercloso* metallaboranes are reported in literature with a range of metal atoms and exohedral ligands.[25] Table 1 summarizes different varieties of *hypercloso* mono-metallaboranes reported in the literature. *Hypercloso* metallaboranes with more than one metal atom[26] are also reported in the literature, but this study is focused only on mono-metallaboranes.

We have estimated the relative stability of the *hypercloso* structures, $C_6H_6MB_9H_9$ (**5**, Figure 4), where M = Fe, Ru, and Os. The transition metal fragments, $(C_6H_6)M$, are considered isolobal to the BH fragment; both are three-orbital and two-electron donors. The relative stability is estimated using the following isodesmic equations:

$$\textit{hypercloso}\text{-}B_{10}H_{10} + \textit{closo}\text{-}1\text{-}\eta^6\text{-}(C_6H_6)\text{-}MB_9H_9^{2-} \rightarrow \textit{closo}\text{-}B_{10}H_{10}^{2-} + \textit{hypercloso}\text{-}1\text{-}\eta^6\text{-}(C_6H_6)\text{-}MB_9H_9 \quad (1)$$

$$\textit{hypercloso}\text{-}B_{10}H_{10} + \textit{closo}\text{-}1\text{-}\eta^6\text{-}(C_6H_6)\text{-}1,3,6\text{-}MC_2B_9H_9^{2-} \rightarrow \textit{closo}\text{-}3,6\text{-}C_2B_8H_{10} + \textit{hypercloso}\text{-}1\text{-}\eta^6\text{-}(C_6H_6)\text{-}MB_9H_9 \quad (2)$$

The reaction energy calculated for eq 1 is exothermic by −61.3, −64.8, and −67.2 kcal/mol for M = Fe, Ru, and Os, respectively. Similarly, reaction 2 is calculated to be exothermic by −39.8, −52.8, and −56.1 kcal/mol for M = Fe, Ru, and Os, respectively. The exothermicity indicates that the *hypercloso* structures are more stable with transition metal fragments, whereas the *closo* structures are more stable with a BH capping group. As the size of the metal atom increases, the exothermicity of the reaction also increases. This indicates the preference of the *hypercloso* structures for the heavier metal fragments with more diffused orbitals versus with the light transition metal fragments. A close look at the experimentally characterized metallaboranes (Table 1) also suggests that the *hypercloso* structures are known mostly with the heavy transition metals at the six-degree vertex versus

(24) (a) Jemmis, E. D. *J. Am. Chem. Soc.* **1982**, *104*, 7017. (b) Jemmis, E. D.; Schleyer, P. v. R. *J. Am. Chem. Soc.* **1982**, *104*, 4781. (c) Jemmis, E. D.; Subramanian, G.; Radom, L. *J. Am. Chem. Soc.* **1992**, *114*, 1481. (d) Srinivas, G. N.; Anoop, A.; Jemmis, E. D.; Hamilton, T. P.; Lammertsma, K.; Leszczynski, J.; Schaefer, H. F., III. *J. Am. Chem. Soc.* **2003**, *125*, 16397. (e) Elian, M.; Chen, M. M. L.; Mingos, D. M. P.; Hoffmann, R. *Inorg. Chem.* **1976**, *15*, 1148. (f) Jemmis, E. D.; Sarma, K. S.; Pavan Kumar, P. N. V. *THEOCHEM* **1985**, *121*, 305. (g) Pathak, B.; Pandian, S.; Hosmane, N.; Jemmis, E. D. *J. Am. Chem. Soc.* **2006**, *128*, 10915. (h) Shameema, O.; Jemmis, E. D. *Angew. Chem., Int. Ed.* **2008**, *47*, 5561.

(25) (a) Hosmane, N. S.; Maguire, J. A. In *Comprehensive Organometallic Chemistry III*; Crabtree, R. H., Mingos, D. M. P., Eds.; Elsevier: Oxford, 2007; Vol. *3*, Chapter 3.05, p 175. (b) Weller, A. S. In *Comprehensive Organometallic Chemistry III*; Crabtree, R. H., Mingos, D. M. P., Eds.; Elsevier: Oxford, 2007; Vol. *3*, Chapter 3.04, p 133. (c) Grimes, R. N. In *Comprehensive Organometallic Chemistry II*; Abel, E. W., Stone, F. G. A., Wilkinson, G., Eds.; Pergamon: New York, 1995; Vol. *1*, p 373.

(26) (a) Lei, X.; Shang, M.; Fehlner, T. P. *Organometallics* **2001**, *20*, 1479. (b) Kim, Y.-H.; Cooke, P. A.; Rath, N. P.; Barton, L.; Greatrex, R.; Kennedy, J. D; Thornton-Pett, M. *Inorg. Chem. Commun.* **1998**, *1*, 375.

(27) Bould, J.; Crook, J. E.; Greenwood, N. N.; Kennedy, J. D.; McDonald, W. S. *J. Chem. Soc., Chem. Commun.* **1982**, 346.

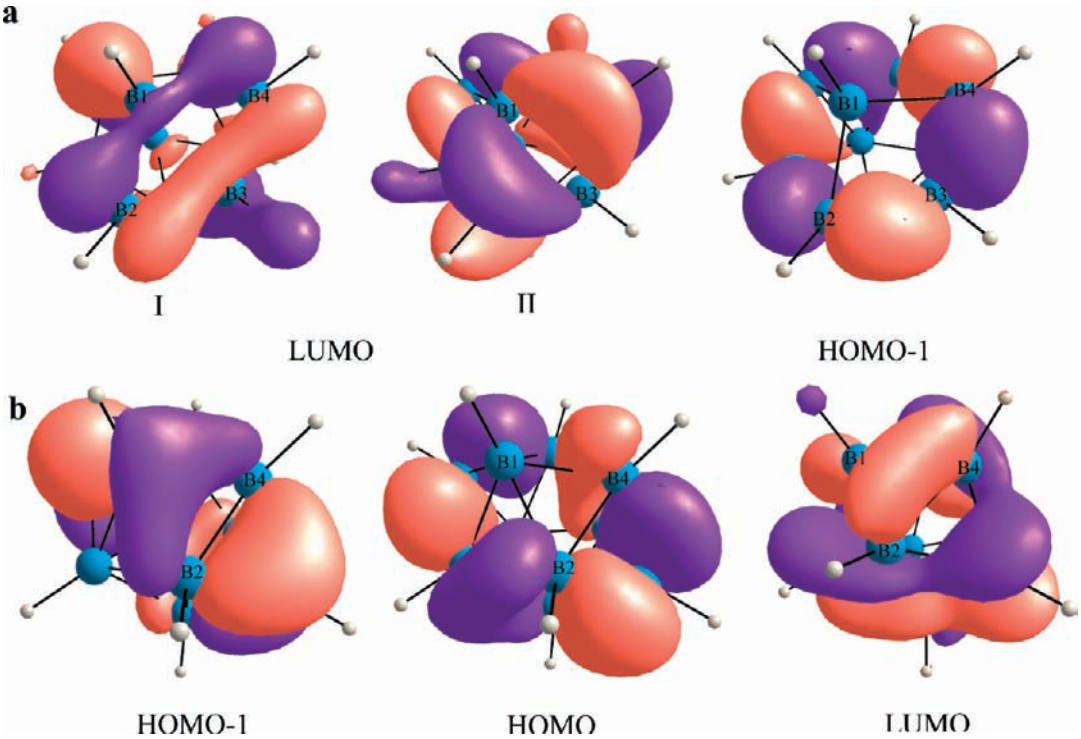

Figure 6. Molecular orbitals of *hypercloso* $B_{10}H_{10}$ (**a**) and *closo* $B_{10}H_{10}^{2-}$ (**b**).

with the light transition metals. We have done further analysis, to show the preference of the heavy transition metal in stabilizing the *hypercloso* geometry over the light transition metal, by considering the following isodesmic equation:

$$\begin{aligned} &\textit{closo}\text{-1-}\eta^6\text{-}(C_6H_6)\text{-1, 3, 6-M}'\text{-}C_2B_7H_9 \\ &+ \textit{hypercloso}\text{-1-}\eta^6\text{-}(C_6H_6)\text{-1-}MB_9H_9 \\ &\rightarrow \textit{closo}\text{-1-}\eta^6\text{-}(C_6H_6)\text{-1, 3, 6-}MC_2B_7H_9 \\ &+ \textit{hypercloso}\text{-1-}\eta^6\text{-}(C_6H_6)\text{-1-M}'\text{-}B_9H_9 \qquad (3) \end{aligned}$$

The reaction is exothermic when a first row transition metal fragment in the *hypercloso* geometry is replaced by a second row transition metal (Table 2). The exothermicity increases when it is replaced by a third row transition metal, indicating the preference of the heavy transition metal fragment in the *hypercloso* geometry over the light transition metal fragment.

Another possible isomer for the *hypercloso* C_6H_6-MB_9H_9, where the metal fragment occupies one of the five-degree vertices and the BH fragment occupying the six-degree vertex is less stable than structure **5** (Figure 4) by 21.2, 24.3, and 26.3 kcal/mol for M = Fe, Ru and Os, respectively. This confirms the preference of the transition metals for the six-degree vertex of *hypercloso* structures.

The Nature of the Exohedral Ligands and the Stability of the *Hypercloso* Structure. The nature of exohedral ligands attached to the metal has an important role in controlling the diffuseness of the frontier orbital of the metal fragment. The smaller the size of the exohedral ligands, the larger will be the diffuseness of metal fragment orbitals. This results in more stable *hypercloso* geometries. We have studied the dependence of the size of the exohedral carbocyclic ring on the stability of the *hypercloso* structure using isodesmic eq 4:

$$\begin{aligned} &\textit{hypercloso}\text{-1-R-}FeB_9H_9 + \textit{closo}\text{-1-R}'\text{-1, 3, 6-}FeC_2B_7H_9 \\ &\rightarrow \textit{closo}\text{-1-R-1, 3, 6-}FeC_2B_7H_9 \\ &+ \textit{hypercloso}\text{-1-R}'\text{-}FeB_9H_9 \qquad (4) \end{aligned}$$

The reaction energy is exothermic by −18.1 and −43.3 kcal/mol for the substitution of $R = C_6H_6$ by $R' = C_5H_5^-$ and $C_4H_4^{2-}$, respectively. Thus, the stability of *hypercloso* geometry increases as the size of the carbocyclic ring decreases for a given metal atom.

(28) (a) Micciche, R. P.; Briguglio, J. J.; Sneddon, L. G. *Inorg. Chem.* **1984**, *23*, 3992. (b) Crook, J. E.; Elrington, M.; Greenwood, N. N.; Kennedy, J. D.; Thornton-Pett, M.; Woollins, J. D. *J .Chem. Soc., Dalton Trans.* **1985**, 2407. (c) Pisareva, I. V.; Chizhevsky, I. T.; Petrovskii, P. V.; Bregadze, V. I.; Dolgushin, F. M.; Yanovsky, A. I. *Organometallics* **1997**, *16*, 5598. (d) Jung, C. W.; Baker, R. T.; Knobler, C. B.; Hawthorne, M. F. *J. Am. Chem. Soc.* **1980**, *102*, 5782. (e) Pisareva, I. V.; Konoplev, V. E.; Petrovskii, P. V.; Vorontsov, E. V.; Dolgushin, F. M.; Yanovsky, A. I.; Chizhevsky, I. T. *Inorg. Chem.* **2004**, *43*, 6228. (f) Ditzel, E. J.; Fontaine, X. L. R.; Greenwood, N. N.; Kennedy, J. D.; Thornton-Pett, M. *Z. Anorg. Allg. Chem.* **1992**, *616*, 79. (g) Kim, Y.-H.; Barton, L.; Rath, N. P.; Kennedy, J. D. *Inorg. Chem. Commun.* **2005**, *8*, 147. (h) Konoplev, V. E.; Pisareva, I. V.; Vorontsov, E. V.; Dolgushin, F. M.; Franken, A.; Kennedy, J. D.; Chizhevsky, I. T. *Inorg. Chem. Commun.* **2003**, *6*, 1454. (i) Bould, J.; Brint, P.; Kennedy, J. D.; Thornton-Pett, M. *J. Chem. Soc., Dalton Trans.* **1993**, 2335. (j) Bould, J.; Greenwood, N. N.; Kennedy, J. D.; McDonald, W. S. *Chem. Commun.* **1982**, 465. (k) Bould, J.; Brint, P.; Fontaine, X. L. R.; Kennedy, J. D.; Thornton-Pett, M. *J. Chem. Soc., Chem. Commun.* **1989**, 1763. (l) Jung, C. W.; Baker, R. T.; Hawthorne, M. F. *J. Am. Chem. Soc.* **1981**, *103*, 810.

(29) (a) Bown, M.; Fontaine, X. L. R.; Greenwood, N. N.; Kennedy, J. D.; Thornton-Pett, M. *J. Chem. Soc., Dalton Trans.* **1990**, 3039. (b) Fowkes, H.; Greenwood, N. N.; Kennedy, J. D.; Thornton-Pett, M. *J. Chem. Soc., Dalton Trans.* **1986**, 517. (c) Fontaine, X. L. R.; Fowkes, H.; Greenwood, N. N.; Kennedy, J. D.; Thornton-Pett, M. *J. Chem. Soc., Dalton Trans.* **1987**, 2417. (d) Ditzel, E. J.; Fontaine, X. L. R.; Greenwood, N. N.; Kennedy, J. D.; Thornton-Pett, M. *Chem. Commun.* **1989**, 1115. (e) Kim, Y.-H.; Cooke, P. A.; Greatrex, R.; Kennedy, J. D.; Thornton-Pett, M. *J. Organomet. Chem.* **1998**, *550*, 341.

Table 1. Experimentally Characterized 9−12-Vertex *Hypercloso* Mono-Metallaboranes and Metallacarboranes

structural formulas	ref
9-Vertex *Hypercloso* Structures	
$[1,1,1\text{-}H(PMe_3)_2(1\text{-}IrB_8H_8)]^a$	
$[1,1,1\text{-}H(PMe_3)_2\text{-}8\text{-}Cl\text{-}1\text{-}IrB_8H_7]^a$	27
10-Vertex *Hypercloso* Structures	
$[1\text{-}\eta^6\text{-}C_6(Me)_3H_3FeB_9H_9]^b$	
$[1,1,1\text{-}(PPh_3)HCl\text{-}1\text{-}RuB_9H_7\text{-}3,5\text{-}(PPh_3)_2]^a$	
$[1\text{-}(pcym)\text{-}RuB_9H_9]^a$	26b
$[2\text{-}Cl\text{-}2,5\text{-}(Ph_3P)_2\text{-}2\text{-}H\text{-}3,9\text{-}(OMe)_2\text{-}2,1\text{-}RuCB_8H_6]^a$	28c
$[2,2\text{-}(Ph_3P)_2\text{-}2\text{-}H\text{-}3,9\text{-}(OMe)_2\text{-}2,1\text{-}RuCB_8H_7]^a$	28c
$[2,3\text{-}(Me)_2\text{-}6\text{-}(CH_2{=}CHCH_2C_6H_4Ph_2P)\text{-}6,2,3\text{-}RuC_2B_7H_7]^a$	28d
$[2,2\text{-}(PPh_3)_2\text{-}2\text{-}H\text{-}3,9\text{-}(OMe)_2\text{-}2,1\text{-}RuCB_8H_7]^a$	28d
$1\text{-}\eta^5\text{-}C_6Me_6\text{-}1\text{-}RuB_9H_9]^b$	28f
$[1\text{-}\eta^6\text{-}C_6Me_6\text{-}2\text{-}(PhNH)\text{-}1\text{-}RuB_9H_8]^a$	28f
$[1,1,1\text{-}(PPh_3)HCl\text{-}5,6\text{-}(PPh_3)_2\text{-}RuB_9H_7]^a$	28g
$[1\text{-}H\text{-}1,1\text{-}(PPh_3)_2\text{-}2\text{-}Ph\text{-}3\text{-}(OMe)\text{-}1,2\text{-}OsCB_8H_7]^a$	28h
$[1,1,1\text{-}(CH{=}CH{-}CH{=}CH)(Ph_2P\text{-}o\text{-}C_6H_4)\text{-}1\text{-}IrB_9H_7\text{-}5\text{-}(PPh_3)\text{-}2\text{-}]^a$	28i
$[1,1,1\text{-}H(PPh_3)(Ph_2P\text{-}o\text{-}C_6H_4)(IrB_9H_8\text{-}2\text{-})]^a$	28j
$[1,1\text{-}(C_6H_4)(Ph_2PC_6H_4)\text{-}1\text{-}IrB_9H_7\text{-}6\text{-}(PPh_3)\text{-}2\text{-}]^b$	28k
$[1,1\text{-}(PEt_3)_2Ru(\eta^6\text{-}C_2B_7H_9)]^b$	28l
11-Vertex *Hypercloso* Structures	
$[1\text{-}\eta^6\text{-}(pcym)\text{-}1\text{-}RuB_{10}H_{10}]^a$	29a
$[1,1\text{-}(PPh_3)_2\text{-}1\text{-}RuB_{10}H_8\text{-}2,5\text{-}(OEt)_2]^a$	28b
$[(P(Me)_2Ph)_2\text{-}1,2\text{-}\mu\text{-}H\text{-}2,5\text{-}(OMe)_2\text{-}1\text{-}RhB_{10}H_8]^a$	29b
$[(P(Me)_2Ph)_2\text{-}1,2\text{-}\mu\text{-}H\text{-}2\text{-}Cl\text{-}5\text{-}(OMe)\text{-}1\text{-}RhB_{10}H_8]^a$	29b
$[1\text{-}\eta^5\text{-}(Me)_5C_5\text{-}1\text{-}RhB_{10}H_{10}]^a$	29c
$[1\text{-}\eta^5\text{-}(Me)_5C_5\text{-}2\text{-}(OMe)\text{-}1\text{-}RhB_{10}H_9]^a$	29c
$[1\text{-}(\eta^5\text{-}(Me)_5C_5\text{-}4\text{-}(NEt_2)\text{-}1\text{-}RhB_{10}H_9]^a$	29d
$[\mu\text{-}1,2\text{-}H\text{-}1,1\text{-}(PPh_3)_2\text{-}2,5\text{-}(OMe)_2\text{-}1\text{-}RhB_{10}H_7]^a$	29b
$[\mu\text{-}1,2\text{-}H\text{-}1,1\text{-}(PPh_3)_2\text{-}2\text{-}Cl\text{-}5\text{-}(OMe)\text{-}1\text{-}RhB_{10}H_7]^a$	29b
$[1\text{-}\eta^6\text{-}(pcym)\text{-}4,4\text{-}(PMe_2Ph)_2\text{-}1,4\text{-}RuPtB_9H_9]^a$	29e
12 Vertex *Hypercloso* Structures	
$[Pt(PEt_3)_2(CO)_2WC_2B_9(CH_2C_6H_4Me)H_8Me_2]^a$	30a
$[l,2\text{-}Ph_2\text{-}5,5\text{-}(CO)_2\text{-}5\text{-}(\eta^3\text{-}C_3H_5)\text{-}5,1,2\text{-}MoC_2B_9H_9]^{-\,a}$	30b

[a] Single crystal XRD data are available. [b] NMR data are available.

Table 2. Reaction Energy in Kilocalories Per Mole for the Isodesmic eq 3

M	M′	ΔE in kcal/mol
Mn^-	Tc^-	−5.4
Mn^-	Re^-	−10.56
Fe	Ru	−13.02
Fe	Os	−16.36
Co^+	Rh^+	−12.86
Co^+	Ir^+	−18.01
Ni^{2+}	Pd^{2+}	−8.47
Ni^{2+}	Pt^{2+}	−12.12

Interaction of the Metal and the B_9H_9 Fragments in the *Hypercloso* Geometry. The interaction between the metal fragment and the B_9H_9 fragment in the *hypercloso* geometry is analyzed using the fragment molecular orbital approach (Figure 7). The most important interaction is the three-level interaction[15d] between the 3e and 4e orbitals of the borane fragment and the 4e orbitals of the metal fragments, which gives a bonding, a nonbonding, and an antibonding MO of the *hypercloso* structure. The

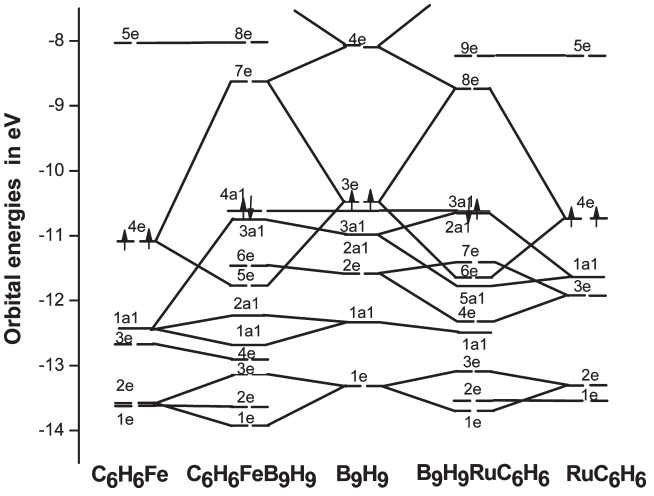

Figure 7. Interaction diagram of the B_9H_9 with $Fe(C_6H_6)$ and $Ru(C_6H_6)$ fragments in the *hypercloso* geometry.

LUMO of the *hypercloso* structure is doubly degenerated. For a *closo* electron count, that is, 11 SEPs, this will lead to the Jahn−Teller distortion of the structure,[15d] resulting in the square antiprismatic *closo* structure. It is also evident from the correlation diagram (Figure 5). Thus, the calculations do not support the argument that a 10-vertex *hypercloso* structure has 11 SEPs. The interaction diagram shows that the metal fragment donates two electrons to cluster bonding. The frontier orbitals of the borane fragment are closer to the frontier orbitals of the $Ru(C_6H_6)$ fragment than those of the $Fe(C_6H_6)$ fragment, which results in the preference of the *hypercloso* geometry by the heavy transition metal fragments. There is, in addition, a contribution from the more diffuse nature of the orbitals of the heavier metal fragment.

Even though $B_{10}H_{10}$ with 10 SEPs does not have a minimum in the *closo* geometry (converges to *hypercloso* geometry), the metallaboranes, $(C_6H_6)MB_9H_9$, have minima in the *closo* geometry. For $(C_6H_6)FeB_9H_9$, the *closo* structure is 22.8 kcal/mol higher in energy than the corresponding *hypercloso* geometry. The *closo* structures are 26.2 and 28.1 kcal/mol less stable than the *hypercloso* structures for $(C_6H_6)RuB_9H_9$ and $(C_6H_6)OsB_9H_9$, respectively. This indicates the stability of *hypercloso* metallaboranes with 10 SEPs and its preference by heavy transition metals.

Interconversion of *Hypercloso* Metallaboranes to *Closo* Metallaboranes. There are several examples for the interconversion of the *hypercloso* to the *closo* structure by reduction. Kennedy et al.[31] reported the reaction of [1-H-1-(PPh_3)-1-(*o*-$Ph_2PC_6H_4$)-*hypercloso*-1-IrB_9H_8] with CS_2, leading to [10-(PPh_3)-2,6;2,9-$(\mu$-$S_2CH)_2$-2-(*o*-$Ph_2PC_6H_4$)-*closo*-IrB_9H_5]. Spencer et al.[32] reported the first example of a chemically reversible and quantitative interconversion of *hypercloso* to *closo* by reducing [1-C_6Me_6-*hypercloso*-1-RuB_9H_9] with sodium dihydronaphthylide into the corresponding square antiprismatic *closo* structure, [2-C_6Me_6-*closo*-2-$RuB_9H_9]^{2-}$. On the

(30) (a) Attfield, M. J.; Howard, J. A. K.; Jelfs, A. N. d. M; Nunn, C. M.; Stone, F. G. A. *J. Chem. Soc., Dalton Trans.* **1987**, 2219. (b) Dunn, S.; Rosair, G. M.; Thomas, R. L.; Weller, A. S.; Welch, A. J. *Angew. Chem., Int. Ed.* **1997**, *36*, 645.

(31) Coldicott, R. S.; Kennedy, J. D.; Thornton-Pett, M. *J. Chem. Soc., Dalton. Trans.* **1996**, 3819.

(32) Littger, R.; Englich, U.; Ruhlandt-Senge, K.; Spencer, J. T. *Angew. Chem., Int. Ed.* **2000**, *39*, 1472.

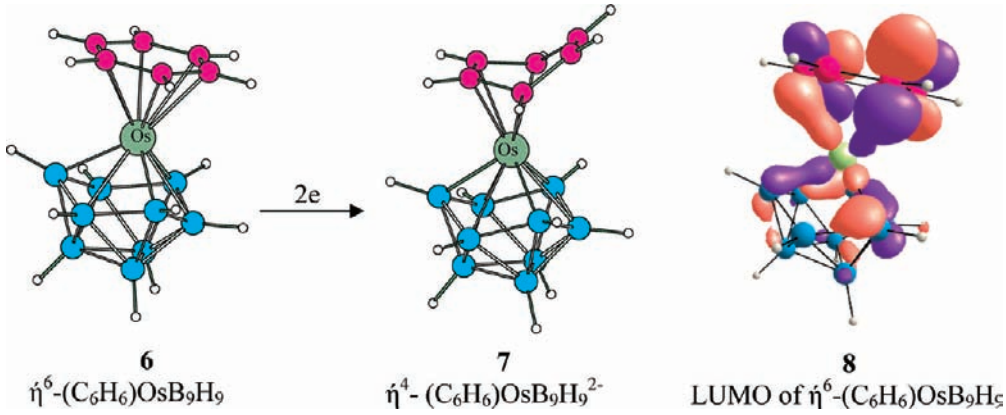

Figure 8. The interconversion of *hypercloso* η^6-$(C_6H_6)OsB_9H_9$ (**6**) to *hypercloso* η^4-$(C_6H_6)OsB_9H_9^{2-}$ (**7**). The LUMO of the *hypercloso* η^6-(C_6H_6)-OsB_9H_9 (**8**).

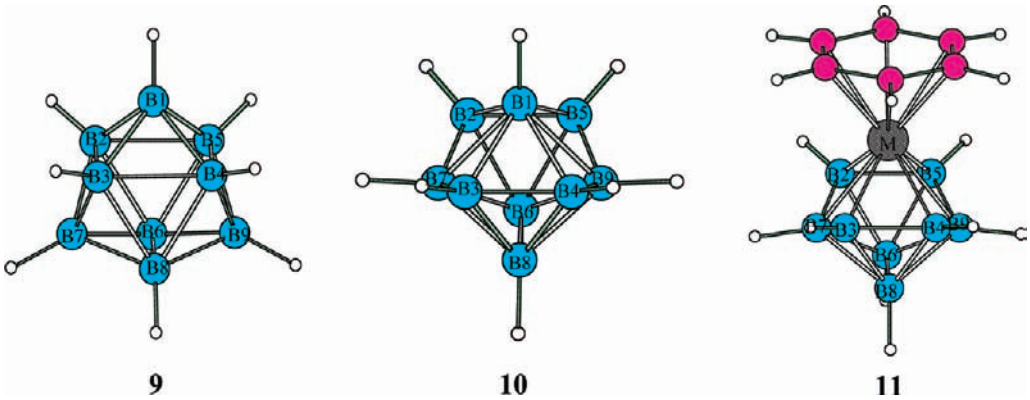

Figure 9. Optimized structures of *closo* $B_9H_9^{2-}$ (**9**), *hypercloso* B_9H_9 (**10**), and *hypercloso* $C_6H_6MB_8H_8$ (**11**).

basis of NMR data, Hawthorne and co-workers postulated[28l] the equilibrium between the *hypercloso* and *closo* RuC_2B_7 clusters as

$$\textit{hypercloso}\text{-}[Ru(PEt_3)_2(\eta^6\text{-}C_2B_7H_9)] + PEt_3 \rightleftarrows \textit{closo}\text{-}[Ru(PEt_3)_3(\eta^5\text{-}C_2B_7H_9)]$$

The *hypercloso* structure is converted to the *closo* structure by the addition of the PEt_3 ligand.

The correlation diagram (Figure S1, Supporting Information) for the interconversion of the *hypercloso* $(C_6H_6)RuB_9H_9$ into the *closo* cluster $(C_6H_6)RuB_9H_9^{2-}$ is quite similar to that of $B_{10}H_{10}$ and $B_{10}H_{10}^{2-}$. There is a large energy difference between the nondegenerate HOMO (A_1) and the doubly degenerated LUMO (E) of the *hypercloso* geometry, indicating the stability of the *hypercloso* geometry. Further addition of the two electrons in the *hypercloso* geometry goes to one of the degenerated LUMOs, which has a bonding interaction between two boron atoms, B1 and B4, and an antibonding interaction between the metal and the boron atom B3 (**5**, Figure 4). The extra added electrons are utilized for forming a B−B bond in the hexagonal face of the B_9H_9 ligand. The stabilization of this orbital results in the transformation of the hexagonal open face of the borane ligand to a pentagonal open face. This coverts the structure from *hypercloso* to *closo* geometry. Similarly, the addition of two electrons into the *hypercloso* $(C_6H_6)FeB_9H_9$ results in the *closo* structure.

The addition of two electrons to the *hypercloso* $(C_6H_6)OsB_9H_9$ does not convert the structure into a *closo* geometry. The B_9H_9 fragment retains the *hypercloso* geometry, whereas the C_6H_6 ring attached to the metal atom changes the coordination from η^6 to η^4 (Figure 8). This indicates that the added electrons are going to the C_6H_6 lignad by distorting it. The structure of the η^4 coordinated C_6H_6 ring is similar to the structure obtained by adding two electrons to the C_6H_6 free molecule. Detailed molecular orbital analysis shows that the LUMO of *hypercloso* $(C_6H_6)OsB_9H_9$ is mainly concentrated on the C_6H_6 ring, and it has antibonding interactions between the carbon atoms, as shown in **8** (Figure 8). In order to decrease the antibonding interaction upon the addition of electrons, the C_6H_6 ring distorts from the planar geometry. The occurrence of the low-lying (C_6H_6) ring orbitals (LUMO) of the *hypercloso* $(C_6H_6)OsB_9H_9$ indicates that the interaction of the metal orbitals with the C_6H_6 ring orbitals is weaker than that with the B_9H_9 fragment orbitals. The *hypercloso*-η^4-(C_6H_6)-$FeB_9H_9^{2-}$ and *hypercloso*-η^4-$(C_6H_6)RuB_9H_9^{2-}$ structures are calculated to be minima, but they are less stable than *closo* structures η^6-$(C_6H_6)FeB_9H_9^{2-}$ and η^6-$(C_6H_6)RuB_9H_9^{2-}$ by 10.3 and 5.6 kcal/mol, respectively. The *hypercloso*-η^4-$(C_6H_6)OsB_9H_9^{2-}$ is calculated to be 5.2 kcal/mol more stable than the *closo*-η^6-$(C_6H_6)OsB_9H_9^{2-}$.

Nine-Vertex *Closo* and *Hypercloso* Metallaboranes. The *closo* $B_9H_9^{2-}$ (C_{3v}) with 10 SEPs has a tricapped trigonal prismatic structure (**9**, Figure 9). It has three four-degree and six five-degree vertices. The *hypercloso* structure B_9H_9 (**10**) with C_{2v} symmetry has one six-degree, four five-degree, and four four-degree vertices. Optimization of the B_9H_9 *hypercloso* structure (**10**) with −2 charges converged to the *closo* $B_9H_9^{2-}$ (**9**). This indicates that nine-vertex *hypercloso* structures require nine SEPs only.

The nine-vertex *closo* and *hypercloso* structures are related by a sequence of two DSD rearrangements. In the *closo* structure (**9**), the B2−B3 (= B5−B4) distance is 1.79 Å and the B1−B7 (= B1−B9) distance is 2.84 Å. In the *hypercloso* structure (**10**), the B2−B3 (= B5−B4) distance is lengthened to 3.0 Å and the B1−B7 (= B1−B9) distance is shortened to 1.91 Å. This creates a six-degree vertex (B1) in the *hypercloso* structure.

The correlation diagram for the interconversion of *hypercloso* to *closo* geometry by the addition of two electrons is shown in Figure 10. The HOMO and LUMO+1 of the *hypercloso* structure have an antibonding interaction between the boron atoms B2 and B3 (= B5 and B4), whereas the LUMO and LUMO+2 have a bonding interaction between B2 and B3 (Figure 11a).

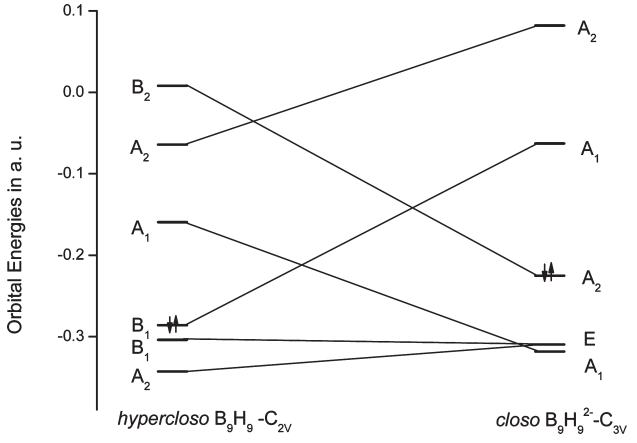

Figure 10. The correlation diagram for the interconversion of the *hypercloso* B_9H_9 to the *closo* $B_9H_9^{2-}$.

The addition of an electron to the *hypercloso* geometry results in the destabilization of the HOMO and LUMO+1 and stabilization of the LUMO and LUMO+2. This results in the shortening of the B2−B3 and B4−B5 distances (3.0 to 1.79 Å) and the elongation of the B1−B7 and B1−B9 distances (1.91 to 2.84 Å). This converts the *hypercloso* structure into the *closo* structure. The interaction of the B_8H_8 fragment with C_6H_6Fe and C_6H_6Ru fragments to form a *hypercloso* structure (Figure S2, Supporting Information) shows that the metal fragment donates two electrons to the cluster bonding in the *hypercloso* structure. The frontier orbitals of the B_8H_8 fragment are closer to the frontier orbitals of the heavy transition metal. This indicates the preference of the *hypercloso* structure for heavy transition metals over light transition metals.

The *closo* structure of B_9H_9 is a minimum which is 23.7 kcal/mol more stable than the *hypercloso* geometry. The presence of the six-degree vertex, B1, in the *hypercloso* structure makes the structure less stable. The *hypercloso* structure can be stabilized by substituting the six-degree vertex with transition metal fragments with largely diffused orbitals. The energy differences between the *closo* and *hypercloso* structures for $C_6H_6MB_8H_8$ are reduced to 8.0, 2.3, and 0.7 kcal/mol for M = Fe, Ru, and Os, which shows the stabilization of *hypercloso* geometry with transition metal fragments. The preference of the heavy transition metal fragment for the *hypercloso* geometry over the *closo* geometry is estimated using the following isodesmic equation:

$$\textit{hypercloso}\text{-}B_9H_9 + \textit{closo}\text{-}1\text{-}\eta^6\text{-}(C_6H_6)\text{-}MB_8H_8^{2-} \rightarrow \textit{closo}\text{-}B_9H_9^{2-} + \textit{hypercloso}\text{-}1\text{-}\eta^6\text{-}(C_6H_6)\text{-}MB_8H_8 \quad (5)$$

The reaction is found to be exothermic by −51.5, −58.7, and −60.5 kcal/mol for M = Fe, Ru, and Os, respectively. Similar to the 10-vertex systems, the exothermicity indicates the stability of *hypercloso* structures with transition metal fragments and the *closo* structure with a BH fragment.

Interconversion of the Nine-Vertex *Hypercloso* Metallaboranes to the *Closo* Metallaboranes. The addition of

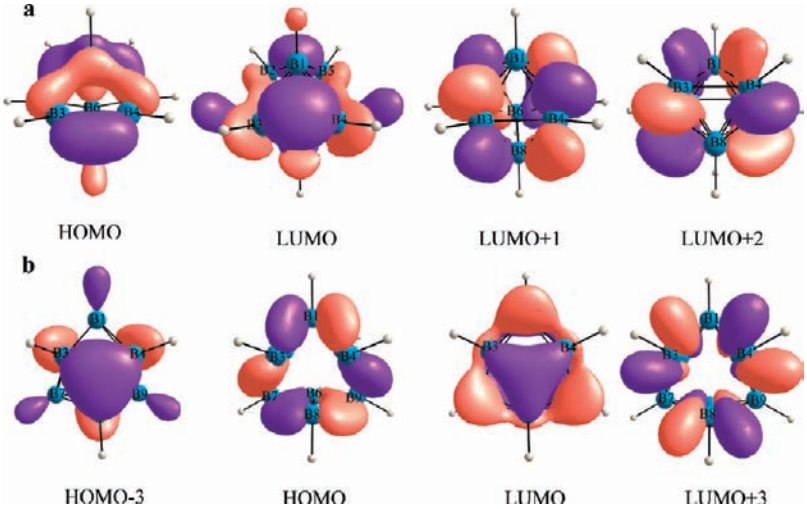

Figure 11. Molecular orbitals of *hypercloso* B_9H_9 (a) and *closo* $B_9H_9^{2-}$ (b).

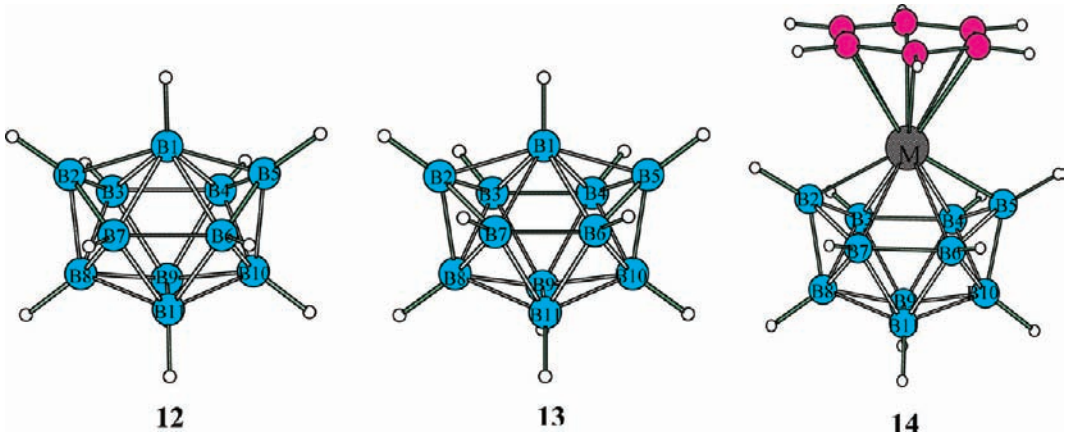

Figure 12. Optimized geometries of *closo* $B_{11}H_{11}^{2-}$ (**12**), *hypercloso* $B_{11}H_{11}$ (**13**), and *hypercloso* $C_6H_6MB_{10}H_{10}$ (**14**).

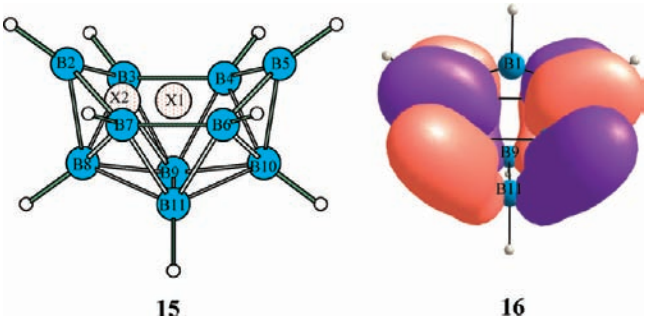

Figure 13. The geometry of the $B_{10}H_{10}$ fragment (**15**) and LUMO of the *hypercloso* $B_{11}H_{11}$ (**16**).

two electrons distorts the nine-vertex *hypercloso* geometry to *closo* geometry. Optimization of the *hypercloso* $C_6H_6FeB_9H_9$ and $C_6H_6RuB_9H_9$ structures with −2 charges converges the structure into the *closo* $C_6H_6FeB_8H_8^{2-}$ and $C_6H_6RuB_8H_8^{2-}$, respectively. The *hypercloso* structure $C_6H_6OsB_8H_8$ retains the *hypercloso* geometry by the addition of a −2 charge. The added electrons go to the C_6H_6 orbitals, resulting in η^4-$(C_6H_6)OsB_8H_8^{2-}$. This indicates the preference of the Os metal with largely diffused orbitals for the *hypercloso* geometry.

The 11-Vertex *Closo* and *Hypercloso* Metallaboranes. The optimized structures of both $B_{11}H_{11}$ (**12**) and $B_{11}H_{11}^{2-}$ (**13**, Figure 12) are topologically the same (C_{2v}) as that of the six-degree vertex which is occupied by a BH fragment.

The $B_{10}H_{10}$ fragment (**15**, Figure 13) to which B1 is capped has a more opened structure in the *hypercloso* geometry than that in the *closo* geometry. This is reflected in the angle X1−X2−B2, which is 136.8° and 145.2° for the *closo* and the *hypercloso* geometry, respectively. The bond distances B7−B6 (= B3−B4) and B7−B2 (= B3−B2 = B6−B5 = B4−B5) are 1.87 and 1.67 Å, respectively, in the *closo* geometry and 1.68 and 1.73 Å in the *hypercloso* geometry. The LUMO of the *hypercloso* $B_{11}H_{11}$ geometry (**16**, Figure 13) has an antibonding interaction between B7 and B6 and a bonding combination between B7 and B2. The addition of an electron to the LUMO results in a shortening of the B7−B2 and a lengthening of B7−B6 bonds. This converts the *hypercloso* structure to the *closo* structure.

The *hypercloso* geometry with a more opened borane fragment can be stabilized more effectively by a transition metal with more diffused orbitals. We have estimated the preference of the heavy transition metal atom over the light metal atom to form a *hypercloso* geometry using the following isodesmic equation:

$$\textit{hypercloso}\text{-}B_{11}H_{11} + \textit{closo}\text{-}1\text{-}\eta^6\text{-}(C_6H_6)\text{-}MB_{10}H_{10}^{2-} \rightarrow \textit{closo}\text{-}B_{11}H_{11}^{2-} + \textit{hypercloso}\text{-}1\text{-}\eta^6\text{-}(C_6H_6)\text{-}MB_{10}H_{10} \quad (6)$$

The reaction is exothermic by −59.9, −61.4, and −59.3 kcal/mol for M = Fe, Ru, and Os, respectively. The change in exothermicity with a change in the metal atom is negligible. It may be due to the fact that the $B_{10}H_{10}$ fragment has an almost similar structure in the *closo* and the *hypercloso* geometry, so that the change of the metal atoms does not make much difference in stability. The interaction diagram (Figure S3, Supporting Information) shows that the metal fragment donates two electrons to the cluster bonding.

The addition of two electrons converts *hypercloso* structures $(C_6H_6)FeB_{10}H_{10}$, $(C_6H_6)Ru\ B_{10}H_{10}$, and $(C_6H_6)OsB_{10}H_{10}$ (**14**, Figure 12) to the *closo* structure. In the case of 10- and 9-vertex forms, the addition of electrons to $(C_6H_6)OsB_9H_9$ and $(C_6H_6)OsB_8H_8$ results in the η^4 coordination of the C_6H_6, retaining the *hypercloso* geometry of the boranes. In the 11-vertex case, since the geometry of the $B_{10}H_{10}$ fragment is quite similar in the *closo* and the *hypercloso* geometry, the addition of electrons converts the structure into the *closo* geometry, by retaining the η^6 coordination of C_6H_6.

The 12-Vertex *Closo* and *Hypercloso* Metallaboranes. The 12-vertex *closo* borane, $B_{12}H_{12}^{2-}$, with I_h symmetry (**17**, Figure 14) has all of the boron atoms at the five-degree vertex. The *hypercloso* borane, $B_{12}H_{12}$, with C_{2v} symmetry (**18**, Figure 14) has two six-degree (B1 and B10), eight five-degree, and two four-degree vertices (B2 and B3). Optimization of the *hypercloso* borane $B_{12}H_{12}$ (**18**) with a −2 charge converges to the *closo* borane (**17**).

The structures of 12-vertex *closo* and *hypercloso* boranes are related by a DSD rearrangement. In the *closo* structure **17**, B2−B3 and B1−B10 distances are 1.79 and 2.89 Å, respectively. In the *hypercloso* geometry (**18**), the

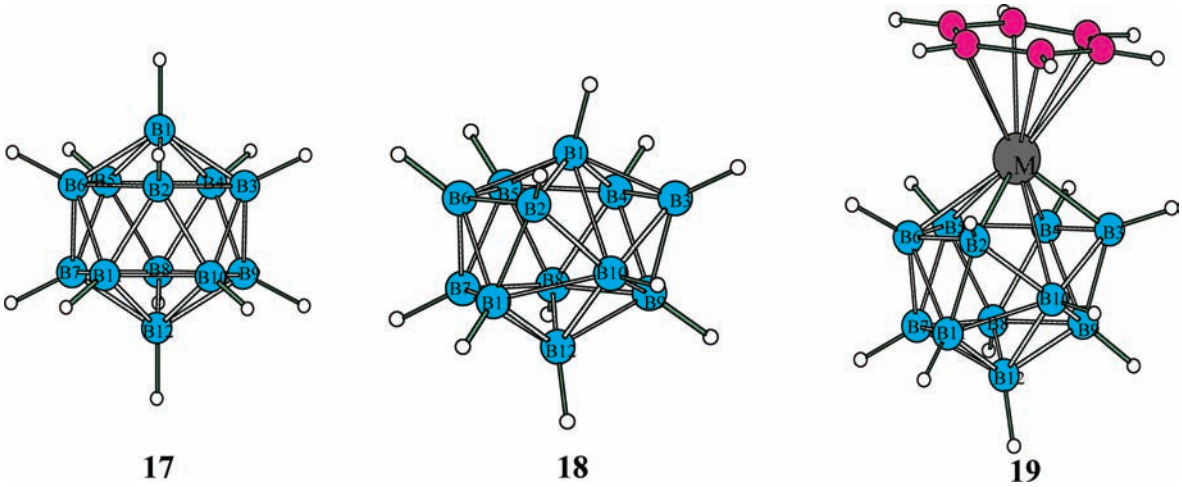

Figure 14. The optimized geometries of *closo* $B_{12}H_{12}^{2-}$ (**17**), *hypercloso* $B_{12}H_{12}$ (**18**), and *hypercloso* metallaborane $C_6H_6MB_{11}H_{11}$ (**19**).

B2−B3 distance is lengthened to 2.78 Å, and the B1−B10 distance is shortened to 2.1 Å. The correlation diagram for the interconversion of 12-vertex *closo* and *hypercloso* boranes by the addition of electrons (Figure S5, Supporting Information) is similar to those of the 11-vertex case, except for the HOMO−LUMO gap of the *hypercloso* structure.

The *hypercloso* borane $B_{12}H_{12}$ can be stabilized by substituting BH groups at the six-degree vertices with transition metal fragments with more diffuse orbitals. As the size of the metal atom increases, the stability of the *hypercloso* structure also will increase. The preference of the heavy transition metal fragment for the *hypercloso* geometry over the *closo* geometry is seen in the exothermicity of the reaction (eq 7), −54.0, −62.8, and −65.2 kcal/mol for M = Fe, Ru, and Os, respectively.

$$\textit{hypercloso}\text{-}B_{12}H_{12} + \textit{closo}\text{-}1\text{-}\eta^6\text{-}(C_6H_6)\text{-}MB_{11}H_{11}^{2-} \rightarrow \textit{closo}\text{-}B_{12}H_{12}^{2-} + \textit{hypercloso}\text{-}1\text{-}\eta^6\text{-}(C_6H_6)\text{-}MB_{11}H_{11} \quad (7)$$

Similar to the cases of 9-, 10-, and 11-vertex systems, the exothermicity indicates the preference for the *hypercloso* structure with metal atoms. Since there are two six-degree vertices in the *hypercloso* $B_{12}H_{12}$ structure (**18**, Figure 14), the structure will be more stable when both the BH groups at the six-degree vertices are replaced by transition metal fragments. The relative stability of the bimetallic *hypercloso* geometry is calculated using the following isodesmic equation:

$$\textit{hypercloso}\text{-}B_{12}H_{12} + \textit{closo}(\text{-}1\text{-}\eta^6\text{-}(C_6H_6)\text{-}M)_2B_{10}H_{10}^{2-} \rightarrow \textit{closo}\text{-}B_{12}H_{12}^{2-} + \textit{hypercloso}\text{-}(1\text{-}\eta^6\text{-}(C_6H_6)\text{-}M)_2B_{10}H_{10} \quad (8)$$

The reaction exothermicity (−108.0, −113.7, and −117.5 kcal/mol for M = Fe, Ru, and Os, respectively) is nearly twice that of the monometallic *hypercloso* systems, indicating that the stabilization by metal substitution is additive for the B_{12} skeleton.

Conclusions

The role of the transition metal in stabilizing the *hypercloso* borane structures with unusual topologies and anomalous electron counts is explored. DFT calculations suggest that *n*-vertex B_nH_n ($n = 9-12$) *hypercloso* structures need only *n* SEPs, but the structures have one or more six-degree vertices. These high-degree vertices can be effectively occupied by transition metal fragments with their highly diffuse orbitals. DFT calculations at the B3LYP/LANL2DZ level on *hypercloso* structures $C_6H_6MB_{n-1}H_{n-1}$ ($n = 9-12$, M = Fe, Ru, and Os) show that a heavy transition metal with more diffuse orbitals is preferred over a light transition metal to form a *hypercloso* geometry. This is further supported by the large number of experimentally characterized *hypercloso* structures with heavy transition metals. The interaction diagram between the borane and the metal fragments in the *hypercloso* geometry shows that the interaction is more effective between a heavy transition metal and a borane fragment. The correlation diagrams for the interconversion of *hypercloso* and *closo* structures show that the addition of electrons to the LUMO of the *hypercloso* structure results in the *closo* structures. The size of the exohedral ligand attached to the metal atom also plays a role in deciding the stability of the *hypercloso* structure.

Acknowledgment. O.S. gratefully acknowledges the Council of Scientific and Industrial Research for a Senior Research Fellowship. The research is supported by the J. C. Bose fellowship of the Department of Science and Technology (DST) and Board of Research in Nuclear Sciences (BRNS). The High Performance Computing Facility (HPCF) funded under the UGC/UPE and DST-FIST programs at the University of Hyderabad and Supercomputer Education and Research Centre (SERC) at IISc provided computational facilities.

Supporting Information Available: Correlation diagram for 10- and 12-vertex *hypercloso* to *closo* metallaborane interconversion; interaction diagram for the 9-, 11-, and 12-vertex *hypercloso* metallaboranes; listing of total energies; and Cartesian coordinates of important structures. This information is available free of charge via the Internet at http://pubs.acs.org.